Impacts of the EA and SCA patterns on the European twentieth century NAO-winter climate relationship

Laia Comas-Bru [a,*] and Frank McDermott [a,b]

[a] School of Geological Sciences, University College Dublin, Dublin 4,Ireland
[b] UCD Earth Institute, University College Dublin, Dublin 4, Ireland
[*] Corresponding author: laia.comas-bru@ucdconnect.ie

Abstract

Much of the twentieth century multidecadal variability in the relationship between North Atlantic Oscillation(NAO) and winter climate over the North Atlantic-European sector can be linked to the combined effects of the NAO and either the East Atlantic pattern (EA) or the Scandinavian pattern (SCA).Our study documents how different NAO-EA and NAO-SCA combinations influence winter climatic conditions (temperature and precipitation) as a consequence of NAO dipole migrations. Using teleconnectivity maps, we find that the zero-correlated line of the NAO-winter-climate relationship migrates southwards when the EA is in the opposite phase to the NAO, related to a southwestwards migration of the NAO dipole under these conditions. Similarly, a clockwise movement of the NAO-winter-climate correlated areas occurs when the phase of the SCA is opposite to that of the NAO, reflecting a clockwise movement of the NAO dipole under these conditions. Our study provides new insights into the causes of spatial and temporal nonstationarity in the climate-NAO relationships, particularly with respect to winter precipitation. Furthermore, interannual variability in the north-south winter precipitation gradient in the UK appears to reflect the migration of the NAO dipole linked to linear combinations of the NAO and the EA. The study also has important implications for studies of the role of the NAO in modulating the wind energy resource of the UK and Ireland, as well as .for the selection of locations for terrestrial proxy archive reconstruction of past states of the NAO.

Received 2 August 2012; Revised 19 December 2012; Accepted 15 March 2013; Published online in Wiley Online Library

Key Words: North Atlantic Oscillation, East Atlantic pattern, Scandinavian pattern, winter precipitation, teleconnection patterns, UK precipitation gradient, CRU-TS3.1, 20CRv2

Citation: Comas-Bru L,McDermott F. 2013. Impacts of the EA and SCA patterns on the European twentieth century NAO-winter-climate relationships. Q.J.R.Meteorol.Soc. DOI:10.1002/qj.2158

1 Introduction

The North Atlantic Oscillation (NAO) is the leading mode of climate variability in the North Atlantic region and is manifest as a meridional dipole anomaly in sea-level pressure (SLP), with the two centres of action located approximately over Iceland (IL) and the Azores (AH) (Hurrell, 1995). It is well known that the NAO exerts a strong influence on air temperature, precipitation and wind patterns over the North Atlantic sector during the boreal winter (Hurrell, 1995; Wanner *et al.*, 2001;

Hurrell *et al.*, 2003). Variability in the strength of this meridional SLP gradient(Figure S3.1 in the online Supporting information) is expressed traditionally as the NAO index (NAOI), defined originally as the simple difference of normalized SLP at meteorological stations located close to the NAO centres of action (e.g. Stykkisholmur (Iceland) and Lisbon (Portugal)(Hurrell, 1995) or Stykkisholmur (Iceland) and Gibraltar (Jones *et al.*, 1997)). The main disadvantages of station based indices are that they are fixed in space, and that they show low signal-to-noise ratios (Hurrell and van Loon, 1997). As a result, most modern NAO indices are derived using linear approaches such as the principal component (PC) time series of the leading empirical orthogonal function (EOF) of regional gridded SLP data (Moore *et al.*, 2013; Wang *et al.*, 2012), or by nonlinear techniques such as cluster analysis (Cassou *et al.*, 2004). In any case, a positive negative) state of the NAO is associated with stronger (weaker) than average westerly winds across the middle latitudes of the Atlantic onto Europe.

The second mode of climate variability in the region, the East Atlantic (EA)pattern, was first described by Wallace and Gutzler (1981) as anomalously high 500 mb height anomalies over the subtropical North Atlantic and eastern Europe when in positive mode. This atmospheric pattern exhibits a well-defined SLP centre of action near 55^oN; 20-35^oW, is also prominent during winter (Barnston and Livezey, 1987), and is known to affect precipitation over the Iberian Peninsula (Rodriguez-Puebla *et al.*, 1998). Moore and Renfrew (2012) derived an EA index (EAI) back to 1870 based on SLP data from Valentia Island (Ireland), but this index has also been defined in the literature as the second leading EOF of regional gridded SLP (Moore *et al.*, 2013).

Following suggestions that the EA pattern may play a role in positioning the primary North Atlantic storm track (Seierstad *et al.*, 2007; Woollings *et al.*, 2010), Moore *et al.* (2011) proposed for the first time that during the positive-NAO winter of 2007, the geographical location of the NAO's centres of action were modulated by other teleconnections, as observed from anomalous occurrences of westerly/easterly tip jet events recorded by in situ climatological and oceanographic data. They found that the two NAO centres of action were displaced to the south (although these conditions are not typically associated with a positive state of the NAO (Hurrell and Deser, 2009)), and they argued further that the phase of the EA plays a role in modulating the location and strength of the NAO dipole. Moore and Renfrew (2012) expanded the former study for the period 1948-2010 using NAO and EA indices derived from SLP data from Iceland and Gibraltar (Jones *et al.*,1997) and Valentia Island (Ireland), respectively.

More recently, another study considered the effect of the Scandinavian pattern (SCA), the third leading mode of winter SLP variability in the European region equivalent to the Eurasia-1 pattern described by Barnston and Livezey (1987), to diagnose the variability in the NAO centres of action (Moore *et al.*, 2013). Moore *et al.* (2013) subsequently investigated these effects by selecting winters that were characterized by different combinations of the NAO-EA and NAO-SCA phases. These authors described a movement of the NAO structure along a northeast–southwest axis depending on the state of the EA, as well as a clockwise/anticlockwise movement associated with the state of the SCA. Figure 1 illustrates the differences in extension and location of the SLP dipole for years where our patterns are in the same phase, $(\text{NAO-EA})_S$ and $(\text{NAO-SCA})_S$, or in opposite phases, $(\text{NAO-EA})_O$ and $(\text{NAO-SCA})_O$. Importantly, the NAO-climate relationship in the European–North Atlantic sector may be affected by these combinations of teleconnection polarities (see section 3).

Following the approach of Moore *et al.* (2013), here we demonstrate for the first time that much of the multidecadal climate variability during the twentieth century in the North Atlantic-European

sector can be linked to specific combinations of NAOI-EAI and NAOI-SCAI signs. In other words, in this study we use the EA and the SCA to diagnose the variable effects of the NAO on the twentieth century European winter climate.

2 Data and methods

2.1 Climate data

We used the recently released high-resolution CRU-TS3.1 data set compiled by the Climate Research Unit (CRU) of the University of East Anglia (Mitchell and Jones, 2005) to assess the relationship of the NAO and the twentieth century (1902-2009) winter climate in the North Atlantic-European land areas (33.25 to 67.25^{o}N and -26.25 to 56.75^{o}E). The CRU-TS3.1 data set comprises 1308 monthly means of interpolated daily values based on the stations available at that time for the period between January 1901 and December 2009, at a regular global spatial resolution of 0.5^{o}x0.5^o over land. The network of meteorological stations on which the CRU-TS3.1 data set is based is shown in Figure S1.1 of the Supporting Information. Since the teleconnection patterns considered in this study are more prominent during boreal winters, consecutive December to February climate data from 1901 to 2009 (108 years; 324 months) were selected to compute winter means. Each winter mean is ascribed to the year of January (i.e. Dec 1981 to Feb 1982 mean is reported as winter 1982) following the common definition for the NAO index (Hurrell, 1995).

Nine climate variables are provided in the data set, two of which are selected for this study: air temperature (^{o}C; *wTmp*) and precipitation (mm; *wPre*).

2.2 Teleconnection indices

The NAO, SCA and EA indices employed here are defined as the three leading vectors of the cross-correlation matrix calculated from monthly SLP anomalies over a confined Atlantic sector (100^{o}E, 10-80^{o}N). We used SLP data from 138 complete winters (DJF; December 1871 to February 2009) from the Twentieth Century Reanalysis data set (20CRv2; Compo *et al.*, 2011), which provides a total of 414 months. Anomalies have been geographically equalized by multiplying them by $\sqrt{cos(\varphi)}$, where φ is the latitude (North *et al.*, 1982). The relative variance in the twentieth century monthly (DJF) SLP field in the region explained by each teleconnection pattern is indicated in Figure 2.

However, caution must be exercised when defining the teleconnection indices using EOF analysis, because the technique may in some cases yield coefficients for the empirical orthogonal weights of incorrect, physically implausible signs. For this reason, it is crucial to ensure that the polarity of the derived EOF time series is consistent with the physical climatic effects described in the literature (Hurrell, 1995; Wanner *et al.*, 2001; CPC, 2012). Here we have fixed the signs of each eigenvector so that the northern pole of the NAO is negative and the main centres of action of the EA and the SCA are positive (Figure 2). As a result, our leading EOF (NAO) is reflected in the SLP field as negative anomalies in the vicinity of Iceland and positive anomalies over the Iberian Peninsula and west of it at 30-40^{o}N (Figure 2(a)), with the zero-line near 50^{o}N over the Atlantic. The second mode, the EA, presents a strong centre of positive SLP anomalies that lies along the nodal line of the NAO dipole at ca. 50^{o}N; 25^{o}W, and a more diffuse centre over northeast Europe (Figure 2(b)). A third centre of action of the EA pattern described by Wallace and Gutzler (1981)southwest of Canary Islands is almost undetectable here. The third leading mode (SCA) shows strong positive SLP anomalies above the Scandinavian countries as well as the UK and Ireland, with a more diffuse centre of opposite sign over Greenland (Figure 2(c)). The additional weaker centre over the Iberian Peninsula and the adjacent Mediterranean and Atlantic described by Barnston and Livezey (1987) in their Eurasia-1 pattern is not evident.

Importantly, our EA and SCA indices are of opposite sign to those presented in Moore *et al.*

(2013); the reader is referred to their figure 2 in contrast with our Figure 2). However, our EA and SCA indices are consistent with others (Wallace and Gutzler, 1981; Moore and Renfrew, 2012; see section S2 of the Supporting Information), and they also yield their expected climatic effects (CPC, 2012). This has important implications because the NAO dipole movements associated with NAO-EA and NAO-SCA combinations suggested by Moore *et al.* (2013) appear to be reversed, and are the opposite of those inferred in this study.

As the orthogonality constraint on the eigenvectors obtained from EOF analysis can lead to problems when ascribing a physical meaning to each eigenvector (the atmospheric patterns that they represent may not be orthogonal), the spatial patterns of our indices were also compared with the four weather regimes presented in Hurrell and Deser (2009): the positive and negative NAO modes, the "Blocking" regime and the "Atlantic Ridge" regime. These weather regimes were originally obtained through cluster-analysis (non-linear technique), and are therefore not constrained by the orthogonality requirement. When visually comparing the impact on the SLP field for each of our three EOF indices (Figure 2) with the different weather regimes (the reader is referred to figure 9 of Hurrell and Deser, 2009), a high degree of resemblance is found between the "Atlantic ridge" regime and the EA pattern (Figure 2(b)) as well as between the "Blocking" regime and the SCA pattern (Figure 2(c)). Consequently, we conclude that these equivalences underpin the physical meaning for the three patterns presented here.

The robustness of our indices has been further verified by checking for consistency with: *(i)* indices compiled from other studies obtained using different techniques; and *(ii)* some pseudo-indices extracted from the 20CRv2 data set (Compo *et al.*, 2011). See discussion in section S2 of the Supporting Information. The results obtained in these comparisons allow us to argue that our three PC-based indices capture similar variability to other published indices.

3 Results

3.1 Effects of the NAO, EA and SCA on winter temperature and precipitation

Figure 3 illustrates the correlation distribution maps between the NAOI, the EAI and the SCAI versus *wTmp* and *wPre* for the complete winters (DJF) between 1902 and 2009 (108 winters). Consistent with previous studies (Hurrell, 1995; Wanner *et al.*, 2001), a positive NAOI is associated with above-normal precipitation in northwest Scotland, northwest Ireland and western Norway, whereas below-normal precipitation is recorded in southern Europe (45-50^{o}N; Figure 3(a)). Simultaneously, warmer winter conditions occur in northern Europe, while colder winters occur in parts of the southern Mediterranean (Figure 3(b)).

When the EAI is positive, above-average precipitation occurs in western Norway, while winter precipitation is lower in much of western Europe(Britain, Ireland, France and the Iberian Peninsula; Figure 3(c)). At the same time, *wTmp* values are lower in the western Mediterranean (Figure 3(d)). Broadly similar climatic effects are found for a positive SCAI, which is associated with below-normal precipitation over western, central and most of northern Europe, with wetter conditions in the Mediterranean, and below-average temperatures across much of Europe, except for northwest Scandinavia, Scotland and Ireland (Figures 3(e) and (f)).

3.2 Spatial stationarity of the NAO-climate relationship

In order to address the crucial question of how the phases of the EA and the SCA in combination with the NAO impact on winter temperature and precipitation patterns in the North Atlantic-European sector, and following the approach of previous workers (Moore *et al.*, 2013), we have divided the data into two subsets for different NAOI-

EAI and NAOI-SCAI sign combinations (Figures 2, 4 and 5). In Figure 4 the non-consecutive years selected for each of these four subsets equally represent the two possible combinations: both indices have the same sign, (NAO-EA)$_S$ and (NAO-SCA)$_S$, or the opposite sign, (NAO-EA)$_O$ and (NAO-SCA)$_O$. First, we will diagnose the effect of these different combinations of signs on the NAO-SLP relationship because changes in the SLP field relative to the 20_{th} century reference position (Figure S3.1 in the Supporting information) are linked to climate variability in the region. When the NAO-EA combination is assessed (left panel of Figure 4), the zero-line of the spatial correlation between winter SLP and the NAOI migrates northwards when both indices are in the same phase, (NAO-EA)$_S$, passing north of Scotland, over southern Scandinavia, crossing the Baltic Sea towards south-eastern Russia (Figure 4(a)). By contrast, when the NAO and the EA are of opposite signs, (NAO-EA)$_O$, the zero-line is shifted southwards, over the Atlantic, crossing Europe over the southern UK and the North Sea coast (Figure 4(c)). The centres of maximum correlation for the latter combination are shifted to the southwest compared with Figure 4(a). On the other hand, the zero-correlation line for the two sets selected according to the SCA phase (right panel of Figure 4) stays over similar latitudes in the Atlantic region (ca. 50^{o}N), but migrates northwards over eastern Europe for winters with the NAO and the SCA in the same phase, (NAO-SCA)$_S$; Figure 4(b), in comparison with (NAO-SCA)$_O$ (Figure 4d), suggesting an anticlockwise rotation of the correlated areas.

The impact of the SLP-NAO relationships discussed above on selected climate variables is illustrated in Figure 5. This diagram reflects broadly similar shifts of the positively/negatively correlated areas shown in Figure 4. Concerning the EA, the change of polarity in the spatial correlations with respect to both wPre and wTmp is shifted northwards for (NAO-EA)$_S$(Figure 5(a) and (e)) compared with (NAO-EA)$_O$(Figure 5(c) and (g)). Winters with NAOI-EAI values of the opposite sign, (NAO-EA)$_O$, show strong spatially coherent *wTmp*-NAOI correlations ($\rho > 0.7$) that extend southwestward across Europe into the Pyrenees and northern Alps (Figure 5(g)). By contrast, when the indices have the same sign,(NAO-EA)$_S$, the region showing strong positive *wTmp*-NAOI correlations is restricted to latitudes above ca. 50^{o}N, and *wTmp*-NAOI for the eastern Mediterranean region becomes negatively correlated (Figure 5(e)). While both *wPre* data subsets show broadly similar correlations with the NAO (Figure 5(a) and (c)), winter precipitation and the NAOI are oppositely correlated in southern Britain and in much of Ireland, depending on the different NAOI-EAI combinations. As a result of this modulation, the NAO's impact on the climate in these regions is not straightforward.

Similar patterns are found for the sets selected according to the phase of the SCA pattern. In terms of *wTmp*, the zero-correlation line is located much further north for (NAO-SCA)$_S$ (Figure 5(f)) winters in comparison with (NAO-SCA)$_O$ (Figure 5(h)). In terms of *wPre*, the negatively correlated area for (NAO-SCA)$_S$ winters extends much further north in eastern Europe (ca. 55^{o}N) and above ca. 60^{o}N in Scandinavia; Figure 5(b)) than for (NAO-SCA)$_O$ winters, when the zero-line moves from ca. 45^{o}N in the west to ca. 50^{o}N in the east (Figure 5(d)). As observed for the EA, *wPre* and *wTmp* are differently correlated to the NAO depending on the concomitant phase of the SCA in regions such as UK, Ireland, and much of northern central Europe.

Since non-consecutive years are selected to compute the correlation maps shown in Figures 4 and 5, there is a need to ensure that the three leading modes of SLP variability in each of the four subsets ((NAO-EA)$_S$, (NAO-EA)$_O$, (NAO-SCA)$_S$ and (NAO-SCA)$_O$) are still represented by the same teleconnection patterns. In other words, we need to check that the leading atmospheric patterns of each subset do not differ from the original NAOI, EAI and SCAI from which they were

derived. To complete this check, new PC-based indices based on approximately half the winters of the original data set have been calculated for each of the four subsets used in Figures 4 and 5. Our results (Figure 6) show that the SLP variability in the non-consecutive years selected to construct the correlation maps in Figures 4 and 5 are representative of the original indices (NAOI, EAI and SCAI), even though the time period used to compute them is approximately half the original data set. Figure S1.2 in the Supporting information depicts the time series of the NAOI, EAI and SCAI and each sub-PCA index. Furthermore, correlation maps similar to those illustrated in Figure 5 are obtained when using the PCA indices computed from the subsets only (not shown).

3.3 Temporal stationarity of the NAO-*wPre* relationship

In order to determine whether the temporal NAO-winter climate relationship is affected by the concurrent phase of the EA and the SCA and to what extent, several multidecadal time-slices have been defined based on NAO-EA and NAO-SCA persistence patterns described in section 3.2 (Figure 7). Here we have used the same periods as those identified previously by Moore *et al.* (2013), even though, as discussed earlier, our EA and SCA indices present different polarities to those computed by them. Thus, the periods 1910-1929 and 1950-1969 (Figures 7(a) and 7(c)) exhibit EA and SCA indices of predominantly opposite sign compared with the NAO, whereas all indices are mainly of the same sign for the periods 1930-1949 and 1970-1989 (Figures 7(b) and 7(d)). The percentage of years that present each sign combination for each of the 20 year period is shown in Figure 7. During the period 1990-2000, each combination accounts for 50% of the years, and hence is not included in our study.

For the remainder of this article we focus on *wPre*, because the NAO-*wTmp* relationship appears to be relatively insensitive to the effect of the EA and the SCA on the concomitant phase of the NAO for the time periods described above (not shown).

Our results (Figure 7) show that winter precipitation in several regions (e.g. Ireland, southern UK and France) is particularly sensitive to different combinations between the NAOI and the coexisting EAI or SCAI. The zero-correlation line defines a more southerly locus, and has a less pronounced northeast-southwest aspect for the 1910-1929 period (Figure 7(a)) compared with the interval 1930-1949 (Figure 7(b)), when more (NAO-EA)$_S$ and (NAO-SCA)$_S$ years occur. For the last two time periods (Figure 7(c) and (d)), there is no predominance of one specific combination of signs over the other, with respect to the SCA, because each possible combination is present in 50% of the winters for 1950-1969 and 1970-1989. As a result, the EA is the dominant influence on the spatial pattern of the NAO-*wPre* correlations for these two periods. The impact of the NAO on the *wPre* in Scandinavia is weaker in a period such as 1950-1969, when the majority of winters have opposing EA and NAO polarities, in comparison with 1970-1989, where 75% of the winters are (NAO-EA)$_S$.

4 Discussion

The spatial non-stationarity of the regional NAO-climate relationships described in section 3.2 can be rationalized on the basis of recent studies of SLP patterns (Moore and Renfrew, 2012) that demonstrated shifts in the NAO centres of actions relative to those used to define the classic station based NAO indices (Hurrell, 1995; Jones *et al.*, 1997) linked to the coexisting states of the EA and the SCA.

As our PC-based NAO index is the projection of the SLP onto a fixed NAO pattern and cannot therefore provide information about the spatial variability of the NAO dipole, teleconnectivity maps (Wallace and Gutzler, 1981) have been used to provide information about the spatial SLP variability associated with the NAO-winter climate correlation maps presented here (Figure 1 and section S3.2 in the Supporting information).

Importantly, the northeastward shift of the Icelandic Low SLP anomalies in the positive NAO regime that can lead to a northward movement of the nodal line of the NAO dipole (Hurrell and Deser, 2009) is not likely to affect our results, because positive and negative states of the NAO are well balanced in all our data subsets.

The teleconnectivity maps (Figure 1) involve shifts in the southern NAO centre of action from the classic locations (Lisbon (Hurrell, 1995), Gibraltar (Jones *et al.*, 1997) and Ponta Delgada (Rogers, 1984)) toward the northeast when the NAO-EA indices have the same sign, $(\text{NAO-EA})_S$. Under these conditions, the southern centre of action migrates to a location west of the Iberian Peninsula and the northern centre is found in the Greenland Sea (Figure 1(a)). By contrast, when the indices are of opposite sign, $(\text{NAO-EA})_O$, the NAO centres of action migrate towards the southwest, resulting in a southern pole west of the Canary Islands and a northern pole between Iceland and Greenland (Figure 1(c)). Thus, the zero-correlation line of the NAOI-climate relationship migrates to lower latitudes when the southern centre of action is located further away from the European continent (Figure 5(c) and (g)). This effect is also noticeable in the location and extent of the areas showing a strong correlation (either positive or negative) between winter SLP and the NAOI (Figure 4(c)).

Similar results are obtained when determining the locations of the NAO centres of action according to different NAOI-SCAI combinations. When these two indices have the same sign, $(\text{NAO-SCA})_S$, the southern node of the NAO is located over France, and the northern pole over northern Greenland (Figure 1(b)). On the other hand, if the SCAI has the opposite sign to the NAOI, $(\text{NAO-SCA})_O$, the southern centre of action migrates towards the southwest, to a location between the Azores and Canary Islands and the northern pole to the southeast in the Greenland Sea (Figure 1(d)). These results suggest that the impact of the phase of SCAI relative to that of the NAOI yields to a clockwise-anticlockwise movement of the NAO dipole, consistent with the migration of the zero-correlation line observed in the NAO-climate correlation distribution maps (Figure 5(b), (f) vs. (d) and (h)) as well as with the spatial correlation maps between SLP and NAO (right panel of Figure 4).

It is also important here to remind the reader that these movements of the NAO centres of action are also described in Moore *et al.* (2013); but because our computed EA and SCA indices have opposite signs (as discussed in section 2.2), the relative movements associated with the Figure 8. Spatial representation of the North Atlantic Oscillation (NAO) centres of action for the 20 year time periods defined in Figure 7: (a) 1910-1929, (b) 1930-1949, (c) 1950-1969 and (d) 1970-1989. Following the approach of Wang *et al.* (2012), the maximum empirical orthogonal weights of the first principal component of sea-level pressure anomalies in each 20 year period over the region 10-80^{o}N, 100^{o}W-40^{o}E yield the location of the centres, the coordinates of which are shown in each panel. The different combinations of NAOI-EAI and NAOI-SCAI described here are the opposite to those presented by Moore *et al.* (2013).

With regard to our analysis of temporal persistence of NAO-EA and NAO-SCA polarities using 20 year time slices, NAO-wPre correlation patterns are consistent with the northeast-southwest migration of the dipole associated with the influence of the EA pattern on the NAO dipole, as well as the clockwise/anticlockwise movement linked to the SCA effect. We have also calculated the locations of the NAO poles for each of these 20 year periods following the approach of Wang *et al.* (2012) (Figure 8). The locations of the SLP dipole, equivalent to the NAO, differ between the selected periods and are consistent with the teleconnectivity maps for these 20 year periods (not shown). For the first two time-slices presented in section 3.3 (Figure 8(a) 1910-1929 and (b) 1930-1949), the northern pole remains at the same location, whereas the southern node mi-

grates northeastwards from near the Azores during 1910-1929 to southwest France in 1930-1949. We argue that this relative movement of the NAO poles reflects the anticlockwise movement of the zero-correlation line observed in 1930-1949 (Figure 8(b)) with respect to 1910-1929 (Figure 8(a)), as well as its northwards migration. Moreover, the SLP dipole is located at its furthest northeastern position for the period 1970-1989, when there is a prevalent $(\text{NAO-EA})_S$ combination of signs. This can be related to the spatial correlation map presented in Figure 7(d), since the high positive correlations seen in western Norway and western Scotland for the period 1970-1989 may be the result of the proximity of the northern NAO node to the European continent. Similarly, both nodes of the SLP dipole are located at their southwesternmost position during the period 1950-1969, when 60% of the 20 year period corresponded to a sign combination of $(\text{NAO-EA})_O$. In addition, the greatest deviation from the classic NAO centres of action is found when the EA pattern is predominantly of the same phase as the NAO (1930-1949 and 1970-1989).

Finally, as an example of how the effects of different NAOI-EAI combinations are manifest on a regional scale, Figure 9 illustrates the mean precipitation anomalies relative to the long-term mean (1902-2009) in the UK and Ireland, for the 14 to 22 winters that show each of the four possible EAI-NAOI sign combinations, calculated from the CRUTS3.1 dataset. With $(\text{NAO-EA})_O$ (Figure 9(a) and (d)), the NAO dipole has migrated to the southwest (Figure 1(c)), and large and spatially coherent negative (positive) precipitation anomalies are found in the UK and Ireland for negative (positive) states of the NAO. By contrast, when $(\text{NAO-EA})_S$ (Figure 9(b) and (c)) the north and south of the UK exhibit opposing precipitation anomaly patterns. We interpret this pattern to reflect the northeasterly migration of the NAO centres of action, as observed with the large-scale patterns depicted in Figure 4(a) and the correlation distribution map shown in Figure 5(a). Under these conditions, the southern NAO pole, located over the Iberian Peninsula, appears to exert a detectable influence on the southern UK and Ireland. Since the north remains relatively unaffected for negative NAO years, the positive precipitation anomalies in the south accentuate the north-south precipitation gradient under negative EAI conditions (Figure 9(c)) in comparison with positive EAI conditions (Figure 9(a)). For positive NAO states, the south of the UK and Ireland experience above-average winter precipitation only in negative EA years. Therefore, a combination of positive NAOI and EAI results in an increased north–south winter precipitation gradient compared with years with negative EA, when wetter conditions are found overall. Of the four possible sign combinations, the steepest north-south gradient is found when the two atmospheric patterns are in their positive modes (Figure 9(b)), confirmed by meteorological observations from Stornoway and Oxford as detailed in Figure 9.

5 Conclusions

Our study demonstrates the important modulating influence of the EA and the SCA on the 20^{th} century winter climate variability, which in turn can be linked to the geographical positions of the NAO dipole. When the NAO and the EA are of the same sign, the NAO centres of action migrate northeastwards, whereas during phases of opposite sign, they move towards the southwest. When the NAO and the SCA show the same sign, the centres of action move in an anticlockwise manner, while when the phases are of opposite sign, there is an anticlockwise rotation. An important implication of these excursions of the NAO dipole is that they influence the spatial and temporal nonstationarity of the NAO-climate relationship. Our results suggest that winter precipitation patterns linked to the NAO are not straightforward in some regions (e.g. southern UK, Ireland and France) because they are influenced by the concomitant state of the EA and SCA. For instance, much of the interannual variability in the UK north-south winter

precipitation gradient discussed in the literature and originally attributed to interannual and interdecadal variations in the NAO (Wilby *et al.*, 1997; Murphy and Washington, 2001) appears to be influenced by these combinations of the NAO and EA.

Our results indicate that the north-south gradient is accentuated by the occurrence of positive EA during positive NAO winters, and is damped during winters with indices of the opposite polarity. The modulating effect of the EA on the NAO may also be relevant to the occurrence of winter droughts in the southern UK, consistent with the severe winter drought of 1976, when our PC-based NAOI and EAI are positive (0.97 and 1.87, respectively), as in Figure 9(b).

Furthermore, the movements of the NAO dipole described in this study are likely to modulate the relationship between the NAO index and wind speed. Since the EA presents a strong centre of action of positive SLP anomalies along the nodal line of the NAO, combinations between NAO and EA phases could affect the strength and latitudinal location of the dominant westerlies entering Europe from the Atlantic. Thus, our study has implications for studies that seek to link wind speed distributions to the state of the NAO, mainly over UK and Ireland (e.g. Brayshaw *et al.*, 2011).

Our study also has important implications for efforts to use a range of climate sensitive proxies, such as tree rings, speleothems, corals and lake sediments to reconstruct the NAOI back through the last few millennia (Goodkin *et al.*, 2008; Trouet *et al.*, 2009; Comas-Bru *et al.*, 2012; Moreno *et al.*, 2012) as some regions may exhibit temporal non-stationarities in the proxy-NAOI relationship.

Acknowledgements

This work was funded by Science Foundation Ireland through the "Research Frontiers Programme" (10/RFP/ GEO2747). We thank Dr. de Barros for his assistance with processing the data sets. The constructive comments of G.W.K. Moore and an anonymous reviewer are also greatly appreciated. We thank Prof. Thuburn, chief editor, and Dr. M.H.P. Ambaum, associate editor, for helpful editorial advice.

Supporting information

Supporting information concerning data analysis and methods is available as part of the online article, as well as the following additional figures and tables:

Figure S1.1. Maps showing the occurrence of at least one meteorological station per grid cell for *wTmp* and *wPre* in the CRU-TS3.1 global data set (Mitchell and Jones, 2005).

Figure S1.2. Comparison of the NAO, EA and SCA indices obtained by EOF analysis using the entire 20CRv2 data set (1902-2009) with new indices obtained by computing another EOF based only on the selected winters.

Table S2.1. Table showing the Spearman Rank coefficient correlations between our three EOF-based indices (NAOI, EAI and SCAI) with a selection of previously published indices and others based on SLP data extracted from the 20CRv2 data set (Compo *et al.*, 2011).

Figure S3.1. Teleconnectivity map of the winter (DJF) monthly SLP field in the North Atlantic region (10-80^{o}N; 100^{o}W-40^{o}E) for the period 1872-2009.

References:

Barnston AG, Livezey RE. 1987. Classification, seasonality and persistence of low-frequency atmospheric circulation patterns. Mon. Weather Rev. 115: 1083-1126.

Brayshaw AD, Troccoli A, Fordham R, Methven J. 2011. The impact of large scale atmospheric circulation patterns on wind power generation and its potential predictability:A case study over the UK. Renew. Energ. 36: 2087-2096.

Cassou C, Terray L, Hurrell JW, Deser C. 2004. North Atlantic winter climate regimes: spatial asymmetry, stationarity with time, and oceanic forcing. J. Climate 17: 1055-1068.

Comas-Bru L, McDermott F, Fleitmann D. 2012. A 1,000 year annually resolved record of speleothem δ^{18}O from Northern Spain; a potential new proxy for North Atlantic Oscillation (NAO) index reconstruction. Geophys.

Res. Abstr. 14: EGU2012-1627-1 (EGU General Assembly, 2012).

Compo GP, Whitaker JS, Sardeshmukh PD, Matsui N, Allan RJ, Yin X, Gleason BE, Vose RS, Rutledge G, Bessemoulin P, Brnnimann S, Brunet M, Crouthamel RI, Grant AN, Groisman PY, Jones PD, Kruk MC, Kruger AC, Marshall GJ, Maugeri M, Mok HY, Nordli Ø, Ross TF, Trigo RM, Wang XL, Woodruff SD, Worley SJ. 2011. The Twentieth Century Reanalysis Project. Q. J. R. Meteorol. Soc. 137(654): 1-28.

CPC. 2012. Northern Hemisphere Teleconnection Patterns. Climate Prediction Centre, US National Oceanic and Atmospheric Administration.http://www.cpc.ncep.noaa.gov/data/teledoc/telecontents.shtml

Goodkin N, Hughen KA, Doney SC, Curry WB. 2008. Increased multidecadal variability of the North Atlantic Oscillation since 1781. Nature Geosci. 1: 844-848.

Hurrell JW. 1995. Decadal trends in the North Atlantic Oscillation: Regional temperatures and precipitation. Science 269: 676-679.

Hurrell JW, Deser C. 2009. North Atlantic climate variability: The role of the North Atlantic Oscillation. J. Mar. Syst. 78: 28-41.

Hurrell JW, van Loon H. 1997. Decadal variations in climate associated with the North Atlantic oscillation. Climate Change 36: 301-326.

Hurrell JW, Kushnir Y, Ottersen G, Visbeck M. 2003. An overview of the North Atlantic Oscillation. In The North Atlantic Oscillation: Climatic Significance and Environmental Impact, Hurrell JW, Kushnir Y, Ottersen G, Visbeck M (eds.). American Geophysical Union: Washington, DC; 1-35.

Jones PD, Jonsson T, Wheeler D. 1997. Extension to the North Atlantic Oscillation using early instrumental pressure observations from Gibraltar and south-west Iceland. Int. J. Climatol. 17: 1433-1450.

Mitchell TD, Jones PD. 2005. An improved method for constructing a database of monthly climate observations and associated high resolution grids. Int. J. Climatol. 25: 693-712.

Moore GWK, Renfrew IA. 2012. Cold European winters: interplay between the NAO and the East Atlantic mode. Atmos. Sci. Lett. 13: 1-8.

Moore GWK, Pickart RS, Renfrew IA. 2011. Complexities in the climate of the subpolar North Atlantic: a case study from the winter of 2007. Q. J. R. Meteorol. Soc. 137: 757-767.

Moore GWK, Renfrew IA, Pickart R. 2013. Multi-decadal mobility of the North Atlantic Oscillation. J. Climate. 26: 2453-2466, DOI:10.1175/JCLI-D-12-00023.1.

Moreno A, Prez A, Frigola J, Nieto-Moreno V, Rodrigo-Gmiz M, Martrat B, Gonzlez-Sampriz P, Morelln M, Martn-Puertas C, Corella JP, Belmonte A, Sancho C, Cacho I, Herrera G, Canals M, Grimalt JO, Jimnez-Espejo F, Martnez-Ruiz F, Vegas-Vilarrbia T, Valero-Garces BL. 2012. The Medieval Climate Anomaly in the Iberian Peninsula reconstructed from marine and lake records. Quat. Sci. Rev. 43: 16-32.

Murphy SJ, Washington R. 2001. United Kingdom and Ireland precipitation variability and the North Atlantic sea-level pressure field. Int. J.Climatol. 21: 939-959.

North GR, Bell TL, Cahalan RF, Moeng FJ. 1982. Sampling errors in the estimation of empirical orthogonal functions. Mon. Weather Rev. 110: 699-706.

Rodriguez-Puebla C, Encinas AH, Nieto S, Garmendia J. 1998. Spatial and temporal patterns of annual precipitation variability over the Iberian Peninsula. Int. J. Climatol. 18: 299-316.

Rogers JC. 1984. The association between the North Atlantic Oscillation and the Southern Oscillation in the Northern Hemisphere, Mon. Weather Rev. 112: 1999-2015.

Seierstad IA, Stephenson DB, Kvamsto NG. 2007. How useful are teleconnection patterns for explaining variability in extratropical storminess? Tellus Ser. A 59: 170-181.

Trouet V, Esper J, Graham NE, Baker A, Scourse JD, Frank DC. 2009. Persistent positive North Atlantic Oscillation mode dominated the Medieval Climate Anomaly. Science 324: 78-80.

Wallace JM, Gutzler DS. 1981. Teleconnections in the geopotential height field during the Northern Hemisphere winter. Mon. Weather Rev. 109: 784-812.

Wang YH, Magnusdottir G, Stern H, Tian X, Yu Y. 2012. Decadal variability of the NAO: Introducing an augmented NAO index. Geophys. Res. Lett. 39: L21702.DOI:10.1029/2012GL053413.

Wanner H, Brnnimann S, Casty C, Gyalistras D, Lutherbacher J, Schmutz CJ, Stephenson DB, Xoplaki E. 2001. North Atlantic Oscillation – concepts and studies. Surv.Geophys. 22: 321-382.

Wilby RL, O'Hare G, Barnsley N. 1997. The North Atlantic Oscillation and British Isles climate variability, 1865-1996. Weather 52(9): 266-275.

Woollings T, Hannachi A, Hoskins B. 2010. Variability of the North Atlantic eddy-driven jet stream. Q. J. R. Meteorol. Soc. 136: 856-868.

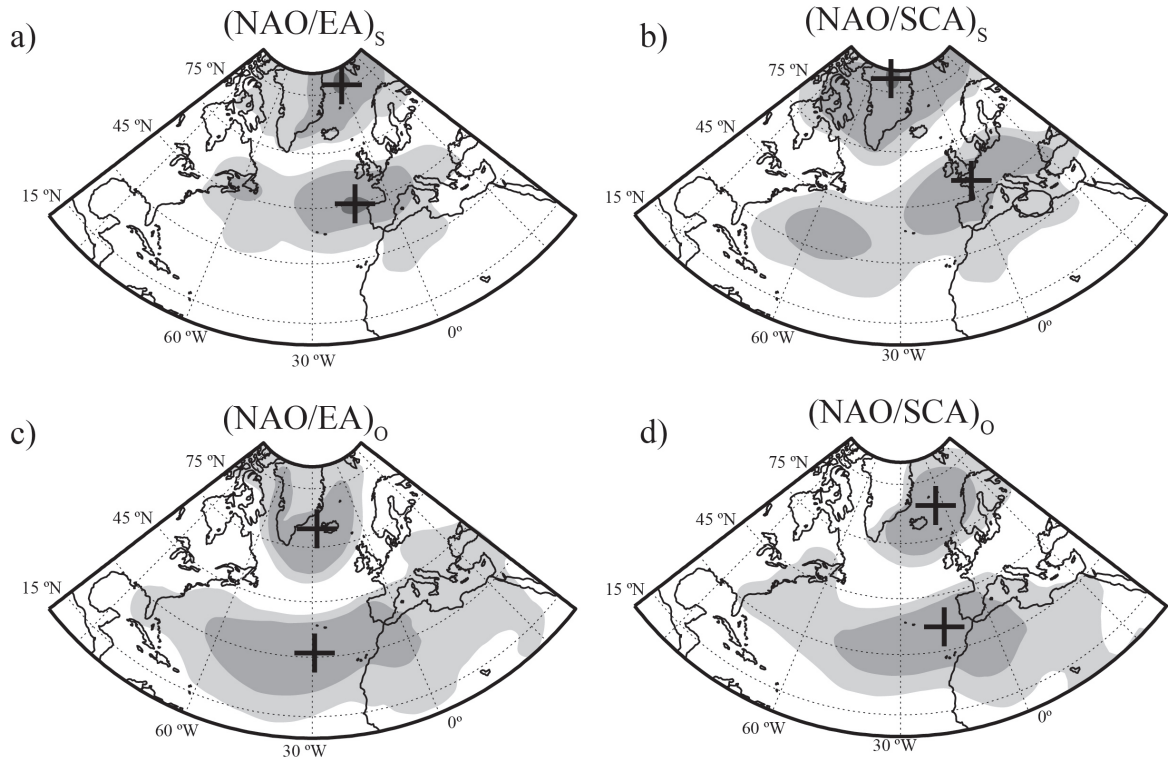

Figure 1: Teleconnectivity matrix of the winter (December-February) monthly sea-level pressure field in the North Atlantic region (10-80N, 100^{o}W-40^{o}E) for the period 1872-2009 for different linear combinations of NAO-EA (left) and NAO-SCA (right). In (a) and (b), both patterns are of the same sign, (NAO-EA)$_S$ and (NAO-SCA)$_S$, whereas they are of opposite signs in (c) and (d), (NAO-EA)$_S$ and (NAO-SCA)$_O$. NAO, North Atlantic Oscillation; EA, East Atlantic pattern; SCA, Scandinavian pattern. Light, medium and dark grey shadings represent areas with correlations of 0.5, 0.6 and 0.7, respectively. Black crosses indicate the location of the highest correlated grid cells. The movements referred to in the text are relative to the 20th century reference period shown in Figure S3.1 in the Supporting information. Please refer to section S3.2 in the Supporting information to see how these maps were constructed.

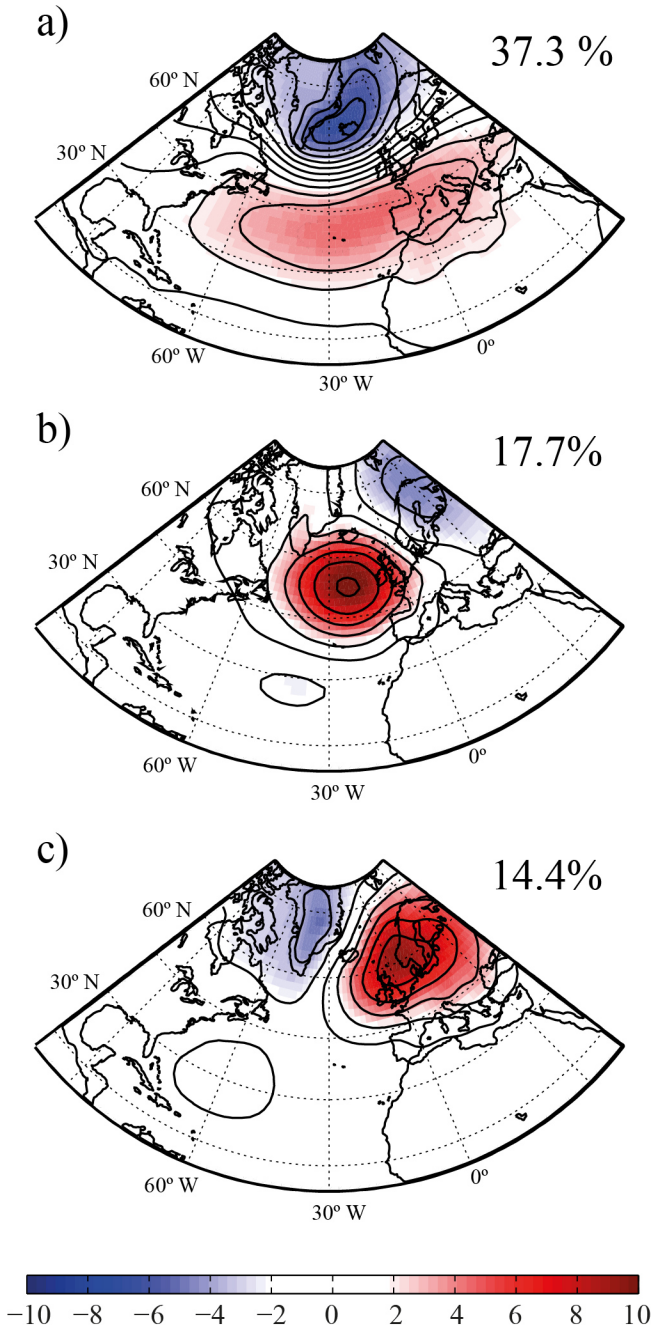

Figure 2: Spatial display of the first three eigenvectors of the gridded winter (December-February) monthly sea-level pressure anomalies (in mb) for the North Atlantic domain (1872-2009) calculated using the 20CRv2 global data set (Compo *et al.*, 2011): (a) North Atlantic Oscillation (NAO),(b) East Atlantic pattern (EA) and (c) Scandinavian pattern (SCA). The empirical orthogonal function was performed using the cross-correlation matrix. Values adjacent to each map are the percentage of the total variance explained by each eigenvector. Please refer to section 2.2 for more information on this analysis.

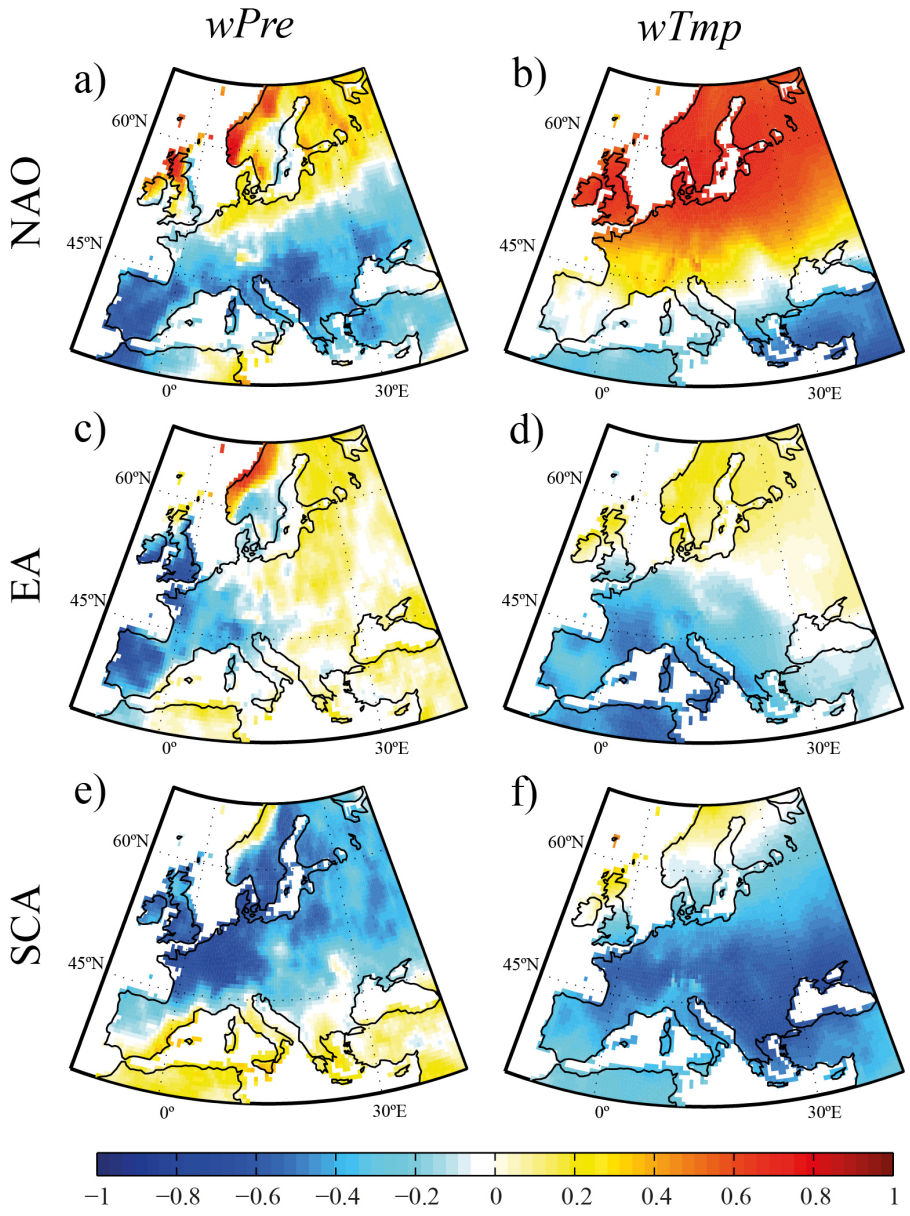

Figure 3: Correlation distribution maps between the winter precipitation and temperature (*wPre* and *wTmp*) data sets and the NAO ((a) and (b)), for the boreal winters (December-February) between 1902 and 2009, calculated using the CRU-TS3.1 global climate data set and our EOF-based indices. Similar correlation distribution maps for ((c) and (d)) EA and ((e) and (f)) SCA. Positive correlations are shown in red and negative correlations are shown in blue (see colour bar). Please refer to section S3.1 in the Supporting information for further details on the Spearman Rank coefficients (ρ). NAO,North Atlantic Oscillation; EA, East Atlantic pattern; SCA, Scandinavian pattern.

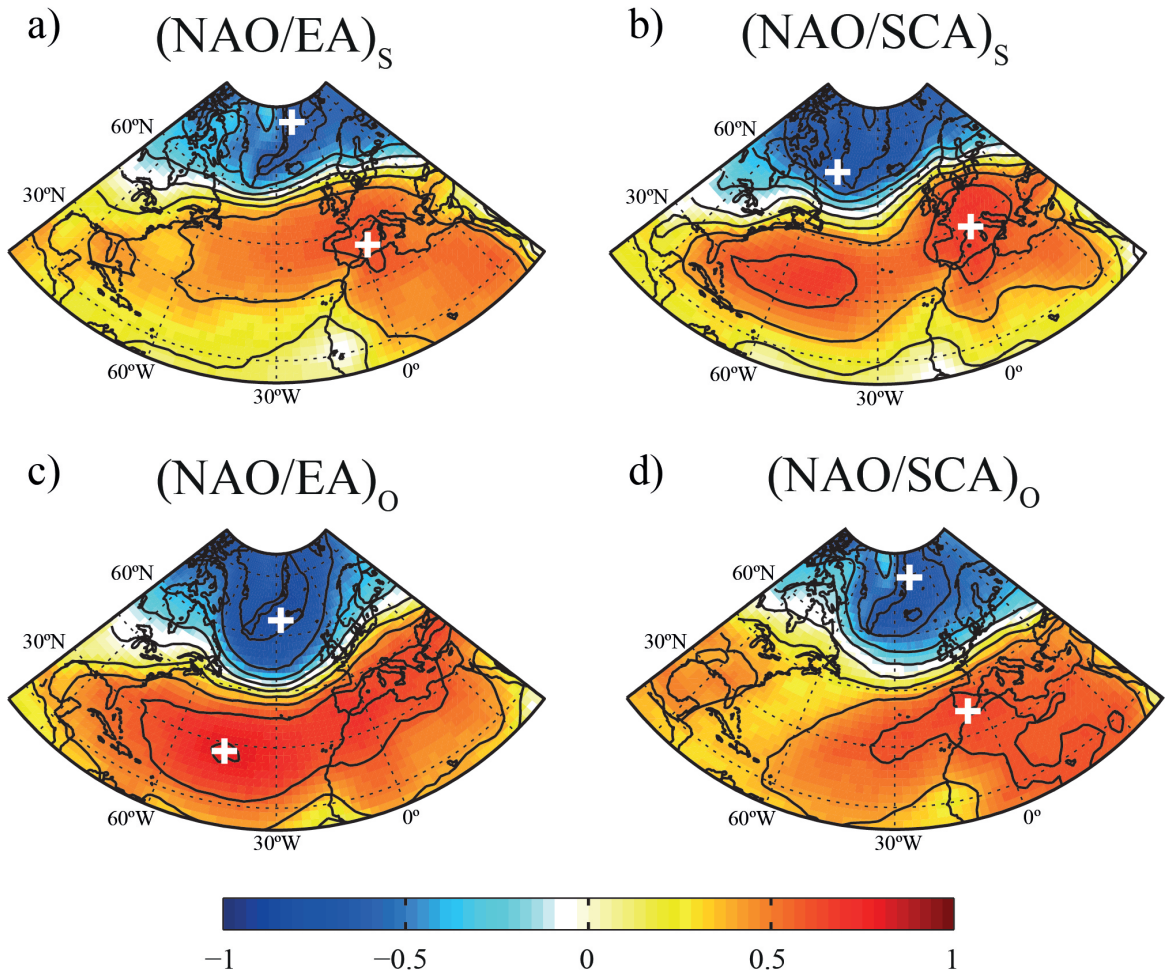

Figure 4: Spatial correlations between winter sea-level pressure and the NAOI for different combinations of the indices: (left) NAOI-EAI combinations based on (a) 51 winters of indices of the same sign, $(\text{NAO-EA})_S$, and (c) 57 winters of different sign, $(\text{NAO-EA})_O$; (right) NAOI-SCAI combinations based on (b) 56 winter of indices of the same sign, $(\text{NAO-SCA})_S$, and (d) 52 winters of different sign, $(\text{NAO-SCA})_O$. NAOI, North Atlantic Oscillation index; EAI, East Atlantic index; SCAI, Scandinavian index. Please refer to the text for further information about the notations. White crosses indicate the location of the strongest correlated grid cells. Correlation coefficients and colour bar as in Figure 3.

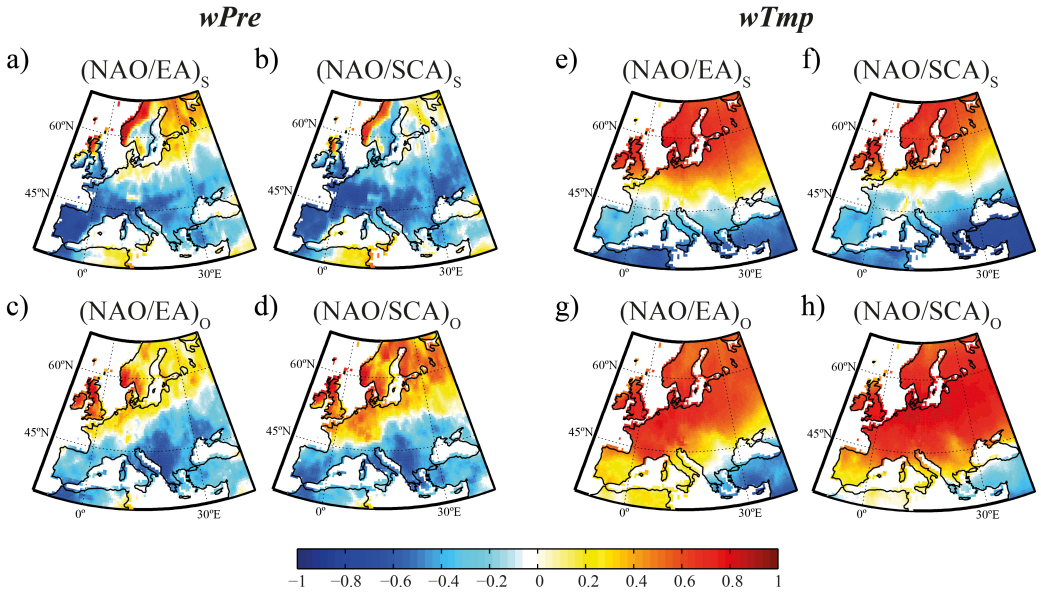

Figure 5: Spatial coherence of the NAO-climate relationship with the CRU-TS3.1 data set and our EOF-based indices, for different combinations of signs: ((a) and (e)) (NAO-EA)$_S$; n = 57; ((c) and (g)) (NAO-EA)$_O$; n = 51; (b,f) (NAO-SCA)$_S$; n = 56 and ((d) and (h)) (NAO-SCA)$_O$; n= 52. NAO, North Atlantic Oscillation; EA, East Atlantic pattern; SCA, Scandinavian pattern. Colour bar, correlation coefficients and notations as in Figure 4.

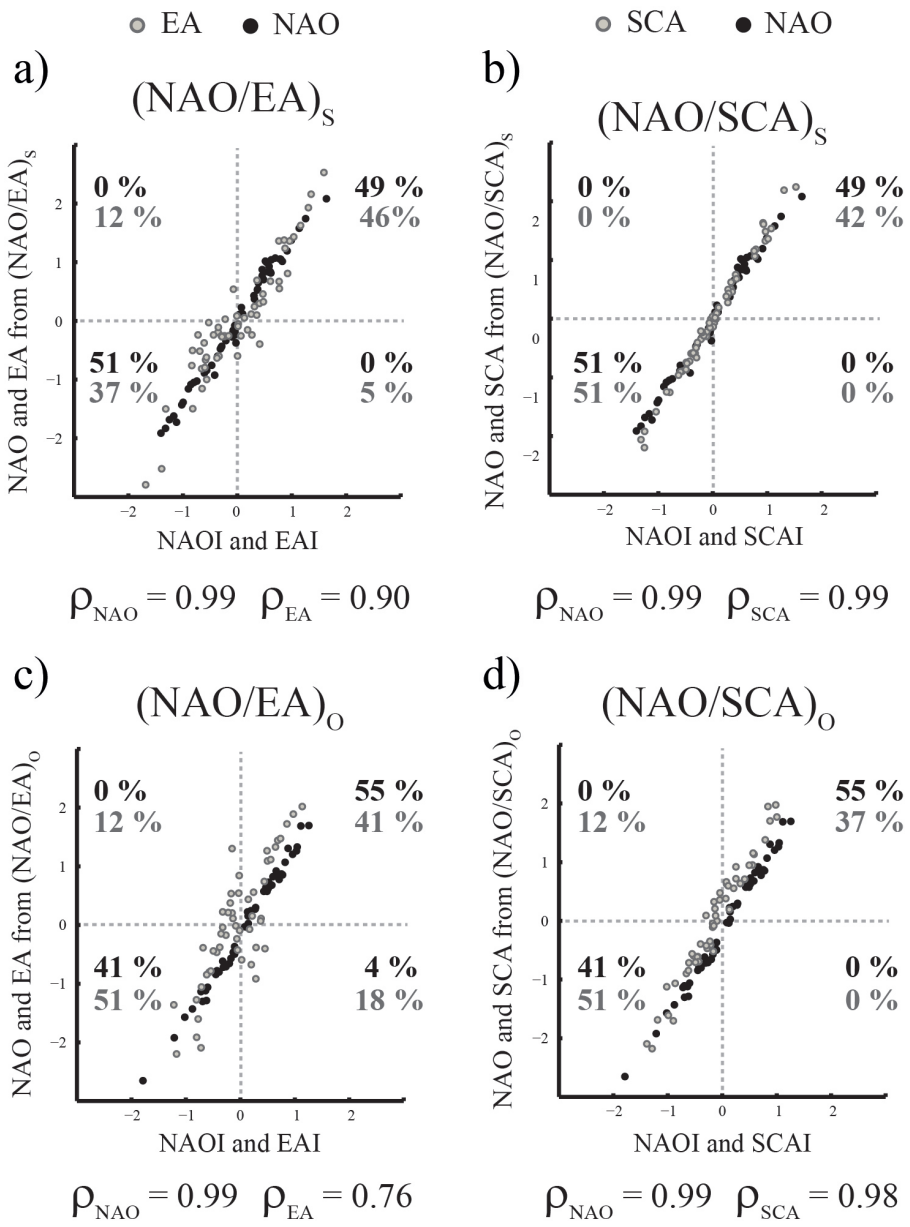

Figure 6: Scatter plots showing our North Atlantic Oscillation, East Atlantic and Scandinavian (NAO, EA and SCA) indices computed by empirical orthogonal function (EOF) analysis from selected subsets of winters that show the same sign: (a) $(\text{NAO-EA})_S$ and (b) $(\text{NAO-SCA})_S$; or different sign: (c) $(\text{NAO-EA})_O$ and (d) $(\text{NAO-SCA})_O$ versus equivalent indices based on EOFs of the entire 20CRv2 data set (1902-2009). Each quadrant represents the same subset shown in Figures 2 and 4. Grey circles represent the ((a) and (c)) EA indices and ((b) and (d)) SCA indices. The NAO indices are represented by black circles. The percentages of winters that fall into each quadrant are indicated in black (top) for the NAO and grey (bottom) for either EA or SCA. The number of winters that correspond to each sign combination is as shown in Figures 4 and 5. Spearman rank coefficient correlations (ρ) between each pair of indices plotted are indicated at the bottom of each scatter plot.

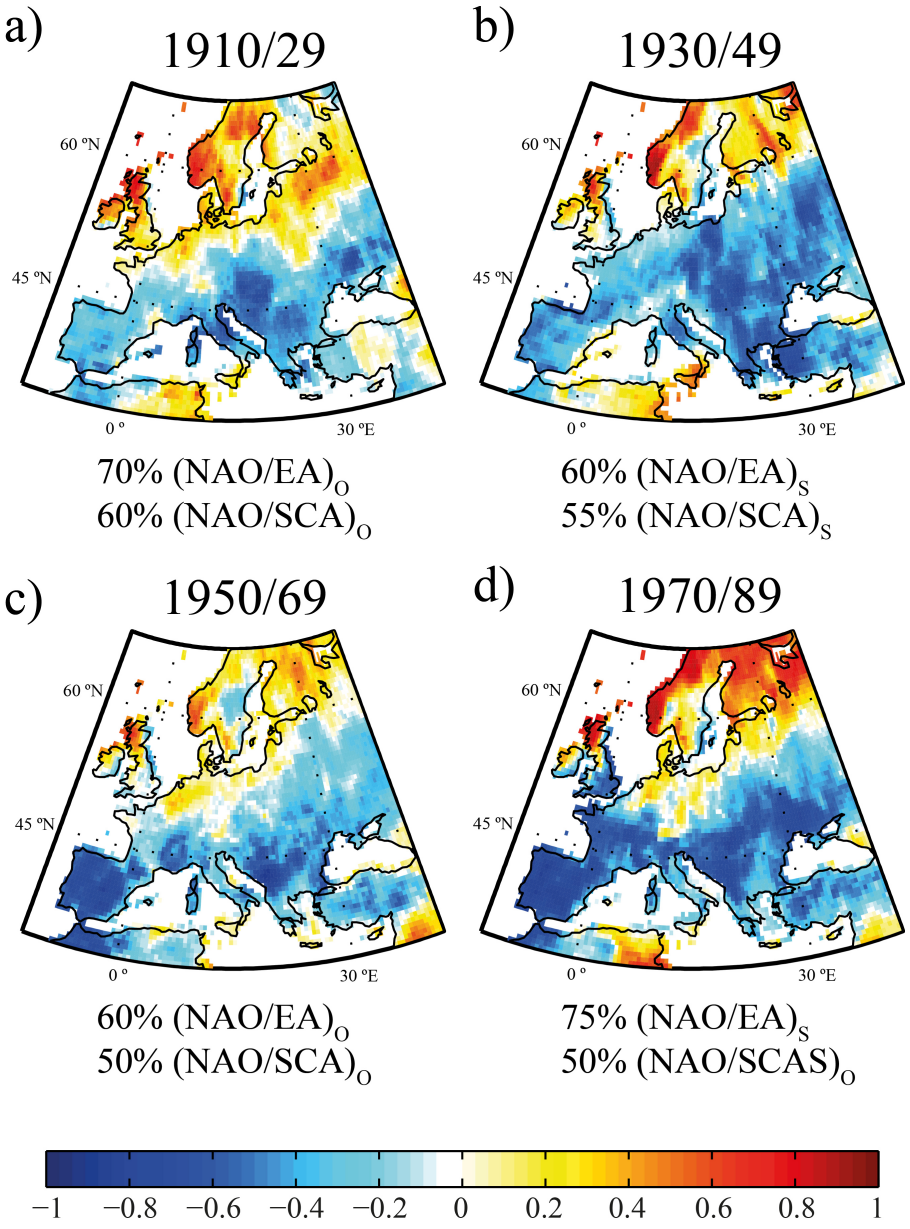

Figure 7: Precipitation data set and North Atlantic Oscillation index (*wPre*-NAOI) correlation distribution maps for 20 year periods: (a) 1910-1929, (b) 1930-1949, (c) 1950-1969 and (d) 1970-1989. These maps have been computed using the CRU-TS3.1 global climate data set and our NAOI based on the first eigenvector of the 20CRv2 sea-level pressure data set. Percentage values beneath each map are the proportion of the years in each period with a given combination of signs. Notations are as on the caption for Figure 1. Colour bar and correlation coefficients as in Figure 3.

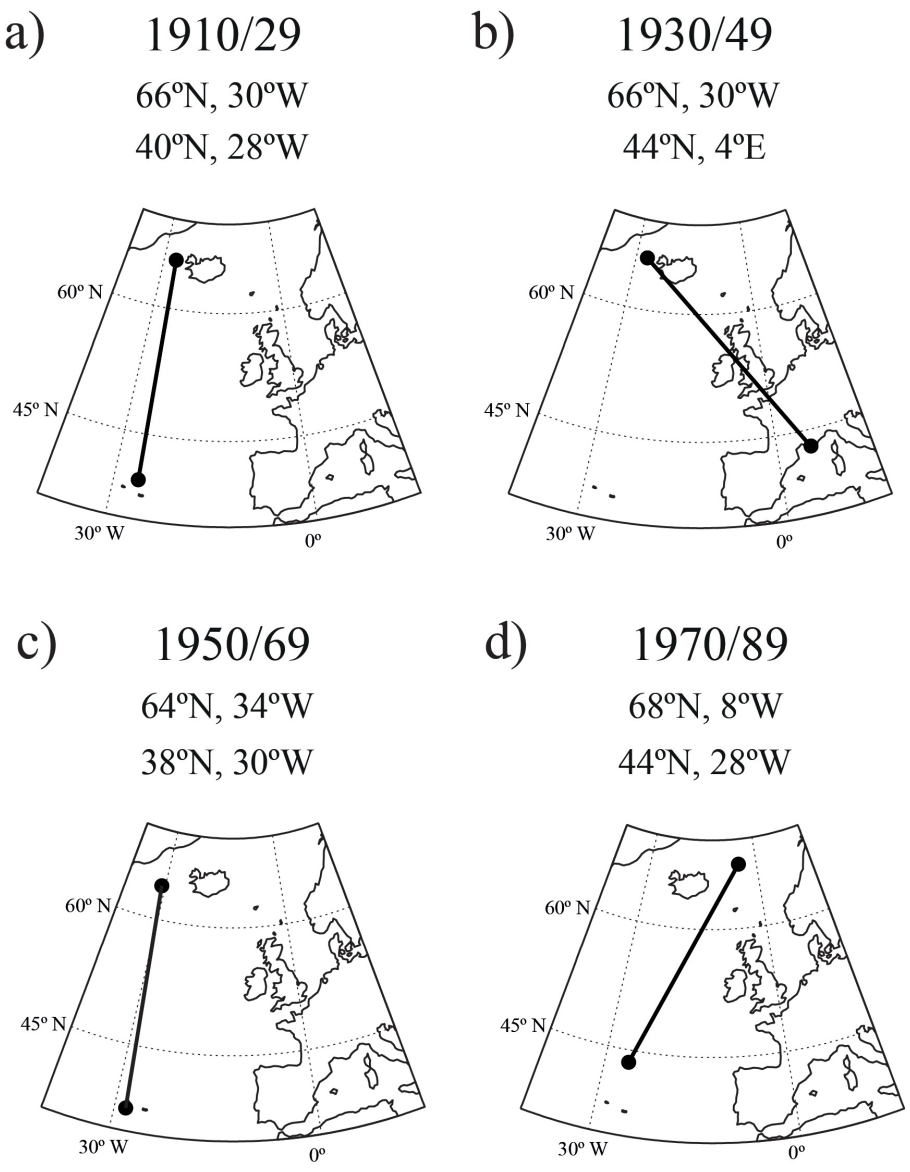

Figure 8: Spatial representation of the North Atlantic Oscillation (NAO)centres of action for the 20 year time periods defined in Figure 7: (a)1910-1929, (b) 1930-1949, (c) 1950-1969 and (d) 1970-1989. Following the approach of Wang *et al.* (2012), the maximum empirical orthogonal weights of the first principal component of sea-level pressure anomalies in each 20 year period over the region 1080^{o}N, 100^{o}W-40^{o}E yield the location of the centres, the coordinates of which are shown in each panel.

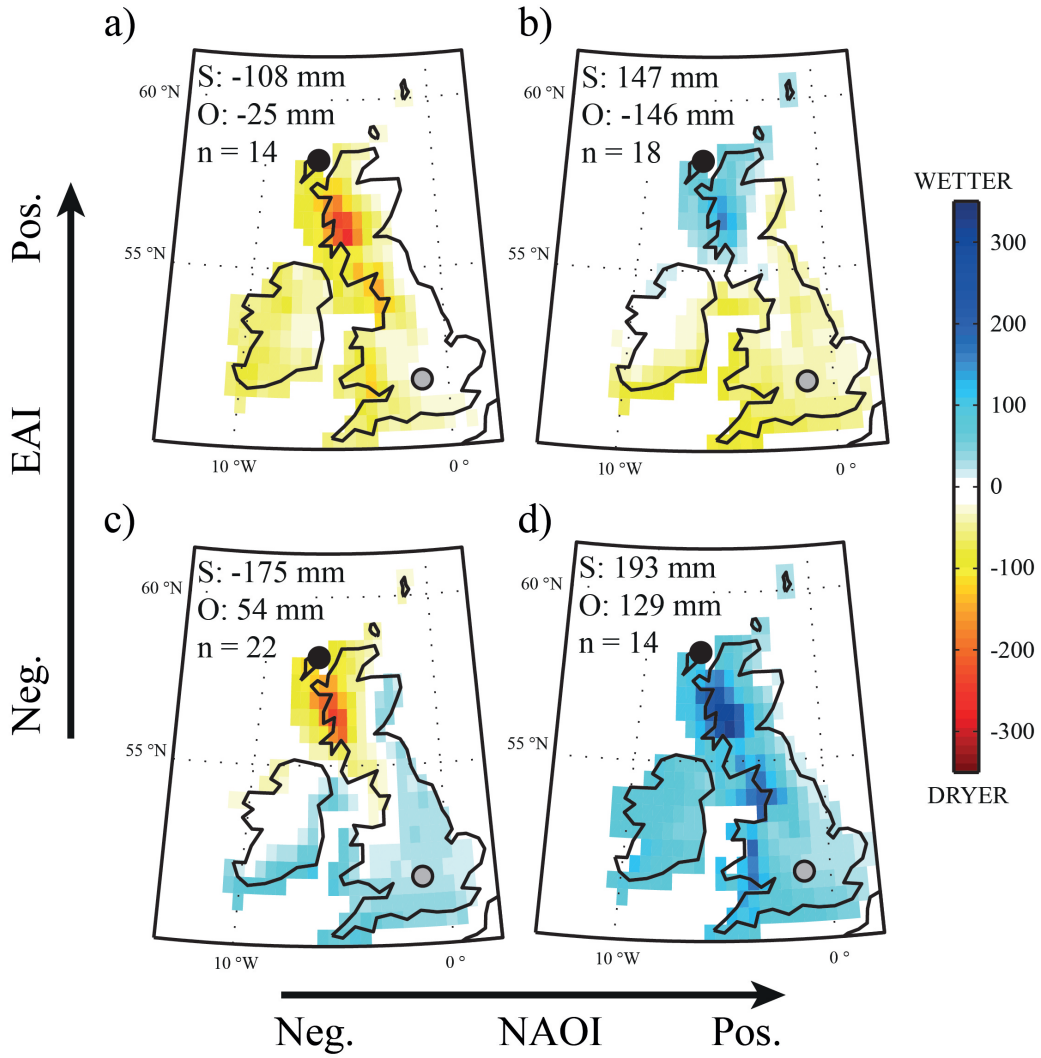

Figure 9: Mean precipitation data set (*wPre*) anomalies (in mm) from the long-term mean (1902-2009) in the UK and Ireland for (a) negative North Atlantic Oscillation index (NAOI) and positive East Atlantic index (EAI), (b) negative NAOI and EAI, (c) positive NAOI and EA and (d) positive NAOI and negative EAI. Winters with NAOI or EAI values within 0.2 of the long-term means have been omitted (n = 27). Also shown are the December-February mean precipitation anomalies for the period 1930-1999 at two selected meteorological stations: Stornoway Airport (S, black circle; 58.33^{o}N, 6.32^{o}W) and Oxford (O, grey circle; 51.77^{o}N, 1.27^{o}W) (available from NOAA Satellite and Information Service (http://lwf.ncdc.noaa.gov/oa/ncdc.html); accessed 22 June 2012). Areas in yellow/red show negative precipitation anomalies and blue areas correspond to positive anomalies (see colour bar).